

Mapping the Interaction between Eukaryotic Initiation Factor 4A (eIF4A) and the Inhibitor Hippuristanol Using Carbene Footprinting and Mass Spectrometry*

James R. Lloyd,¹ Amy Hogan,^{1†} Vasileios Paschalis,^{1,2} Jeddiah Bellamy-Carter,^{1,3} Andrew Bottley,⁴ Graham B. Seymour,⁴ Christopher J. Hayes,¹ and Neil J. Oldham¹

1. School of Chemistry, University of Nottingham, University Park, Nottingham, NG7 2RD, UK
2. Current address: Department of Molecular and Cell Biology, University of Leicester, University Road, Leicester, LE1 7RH, UK
3. Current address: School of Biosciences, University of Birmingham, Birmingham, B15 2TT, UK
4. School of Biosciences, University of Nottingham, Sutton Bonington Campus, Sutton Bonington, Leicestershire, LE12 5RD, UK

* Dedicated to the memory of Amy Hogan, who made a valuable contribution to this work as part of her undergraduate research project. She is sadly missed by all who knew her.

† Deceased

Abstract:

Protein-ligand interactions are central to protein activity and cell functionality. Improved knowledge of these relationships greatly benefits our understanding of key biological processes and aids in rational drug design towards the treatment of clinically relevant diseases. Carbene footprinting is a recently developed mass spectrometry-based chemical labelling technique that provides valuable information relating to protein-ligand interactions, such as the mapping of binding sites and associated conformational change. Here we show the application of carbene footprinting to the interaction between eIF4A helicase and a natural product inhibitor, hippuristanol, found in the coral *Isis hippuris*. Upon addition of hippuristanol we identified reduced carbene labelling (masking) in regions of eIF4A previously implicated in ligand binding. Additionally, we detected hippuristanol-associated increased carbene labelling (unmasking) around the flexible hinge region of eIF4A, indicating ligand-induced conformational change. This work represents further development of the carbene footprinting technique and demonstrates its potential in characterising medically relevant protein-ligand interactions.

Statement of Significance of the Study

This work shows that carbene footprinting can be applied to mapping the binding site of the small molecule inhibitor hippuristanol on the helicase eIF4A, which is a potential target for medicinal intervention. Beyond identifying the direct site of interaction, the methodology also reveals conformational changes associated with the interaction. This provides a platform for identifying the mode of action of novel eIF4A inhibitors.

1 Introduction

Biophysical analysis of protein-ligand interactions and, in particular, structural interrogation of these complexes is a prerequisite to increased understanding of biology at the molecular level and an important stage of drug discovery [1]. There are a range of tools available for the study of protein-ligand interactions that each possess their own advantages and limitations. X-ray crystallography has long been a cornerstone of structural biology and can provide atomic-level information about protein structure [2]. Nevertheless, the technique is time consuming, requires relatively large amounts of sample and, furthermore, some proteins may not be amenable to crystallisation. Nuclear magnetic resonance (NMR) spectroscopy has also proven invaluable in characterising protein-ligand interactions, owing to its high spatial and temporal resolution [3]. Over the last 25 years, mass spectrometry (MS) has emerged as a powerful complementary technique to interrogate noncovalent interactions of biological macromolecules providing valuable information such as binding site locations, dissociation constants, binding stoichiometry and conformational changes resulting from interaction [4]. The speed and sensitivity of MS makes it amenable to higher throughput with lower sample consumption.

MS-based chemical labelling strategies, including hydrogen-deuterium exchange (HDX) [5, 6, 7], hydroxyl radical protein footprinting (HRPF) [8, 9, 10] and carbene footprinting [11] use chemical reagents to identify changes in accessibility of a protein's surface and thereby highlight protein-ligand binding sites. The incorporation of chemical reagents to accessible residues is usually carried out in the presence and absence of a binding partner to provide a differential experimental design [12]. A bound ligand will shield a region of a protein from chemical modification, while unbound sites remain accessible for labelling. These methods all share a similar generalised bottom-up proteomics workflow where digestion and LC-MS stages are subsequently employed to determine the difference in peptide labelling between ligand-treated and control samples. This can be converted to topographical information by plotting changes in labelling on the surface of a protein structure [13].

Carbene footprinting is a relatively recently developed covalent labelling technique which exploits the inherent reactivity of carbenes to react on a nanosecond to microsecond timescale. This irreversibly labels proteins and leads to a detectable mass shift [14].

Carbenes can be generated in several ways but the photolysis of diazirines by irradiation in the near-UV region is particularly convenient. The sodium salt of the aryldiazirine 4-(3-(trifluoromethyl)-3H-diazirin-3-yl)benzoic acid (TDBA) is now an established precursor used in carbene footprinting experiments [15]. Prior to carbene formation, polar and nonpolar groups aid solubility and non-covalent interaction with amino acid side-chains without perturbing protein structure. Irradiation of TDBA at 349 nm yields the carbene, outside of the absorbance region of aromatic amino acids. Covalent insertion of the carbene generates a mass shift of 202.14 Da, and an LC retention time shift of minutes, making the modified peptide easy to recognise [16]. The recent development of PepFoot, a piece of inhouse-built software designed for the semi-automated quantification of covalent labelling, has improved the accuracy and speed with which data from carbene footprinting experiments are analysed [17].

Carbene Footprinting has been used to label several protein systems successfully, for example, the technique was employed to identify the interaction site of the gladiolin polyketide synthase subunits GbnD4 DHD and GbnD5 DH [18], the ubiquitin binding domains of the ubiquitin specific protease USP5, and the binding cleft of hen egg white lysozyme [15]. Lu and colleagues explored footprinting

at the subs residue level to gain insight into how the estrogen-related receptor α (ERR α) interacted with potential agonists [19].

The eukaryotic initiation factor 4A (eIF4A) is a member of the DEAD-box family of helicases involved in displacing bound proteins and unwinding the 5' untranslated region (5' UTR) of mRNA during translation [20]. The eIF4A family is comprised of three related proteins: eIF4AI (DDX2A), eIF4AII (DDX2B) and eIF4AIII (DDX48) [21]. eIF4AI and eIF4AII display 90% sequence similarity however only eIF4AI is required for cell viability. eIF4AI is also more abundant in cells and the most well characterised form of the protein [22]. The third paralog, eIF4AIII, is involved in exon junction complexes and only shares ~67% sequence similarity to eIF4AI [23].

eIF4A is a dumbbell-shaped protein which features two RecA-like domains joined by an intermediate, flexible linker [24, 25]. Conserved motifs line these domains and contribute to mRNA and ATP binding (Figure S1.) [26]. The protein is conformationally dynamic: in the absence of mRNA and ATP, eIF4A occupies an open structure with no inter-domain contact however their binding prompts closure of the protein which promotes contact with conserved residues [27]. The closed state is transiently occupied and ATP hydrolysis is linked to displacement of mRNA-bound proteins and removal of secondary structures in mRNA, as well as release of mRNA and restoration of the protein's open unbound structure [27]. This conformational cycling between open and closed states is key to eIF4A activity [28].

eIF4A makes up the eIF4F complex with two other proteins, eIF4E and eIF4G. eIF4E is a 5'-mRNA cap-binding protein and eIF4G is a scaffolding protein which associates eIF4A and eIF4E subunits [29]. After interaction of the mRNA 5' cap with eIF4E in eIF4F, eIF4A serves to remove secondary structures from mRNA, further stimulated by eIF4B and eIF4H activity (Figure 1) [30]. The ribosome is thought to display some mRNA unwinding activity however stable mRNA structures require the assistance of eIF4A [31]. The 43S pre-initiation complex – formed of the 40S ribosomal subunit, eIF3 and a ternary complex containing tRNA methionine-initiator, eIF2 and GTP – associates with the eIF4F complex and scans the 5' UTR towards the start codon [32]. The 60S ribosomal subunit is then recruited at the start codon and the 80S ribosome is primed for translational elongation [32].

Hippuristanol is a polyoxygenated steroid sourced from the coral *Isis hippuris* and a promising inhibitor of the early stages of protein synthesis [33]. NMR experiments on the C-terminal domain of eIF4A have suggested that hippuristanol binds directly to several conserved residues within this region of the protein [34, 35]. Mutagenesis studies have further reinforced the importance of these residues in binding [34]. Furthermore, studies using single-molecule Förster resonance energy transfer (FRET) experiments have suggested that interaction with hippuristanol maintains full-length eIF4A in a closed conformation, consequently preventing mRNA, but not ATP, from binding the protein [36]. The use of hippuristanol to inhibit eIF4A selectively and consequently stall translation initiation is an attractive strategy for targeting human cancers. Indeed, hippuristanol's anti-neoplastic activity is well-documented and demonstrates the potential for targeting eIF4A/eIF4F in tumour cells [37, 38, 39].

Here we apply carbene footprinting of full-length eIF4A to map the interaction site of hippuristanol and examine the effect of binding upon the protein's structure.

2 Materials and methods

All chemicals and reagents were purchased from Sigma-Aldrich or Thermo Fisher Scientific, unless specified otherwise.

Expression and purification of eIF4A

The DNA coding 6xHis-TEV-eIF4A (optimised for *E. coli* K12) was synthesised by DC Biosciences (Dundee, UK) and inserted into pET32a between the *NdeI* and *XhoI* sites to obtain pET32a-eIF4A (TrxA-His6-TEV-eIF4A). The pET32a-eIF4A expression plasmid was transformed into BL21 (DE3) Rosetta *E. coli*. The cells were cultured in 2xYT media supplemented with 50 µg / ml carbenicillin at 37°C until mid-log phase ($OD_{595} = 0.8$) followed by incubating at 4°C for 10 minutes. 6xHis-TEV-eIF4A expression was induced with 1 mM IPTG (isopropyl-thiogalactopyranoside) for 3 hours at 25°C. The cell pellet was harvested by centrifugation at 3000 g for 15 minutes at 4°C and suspended in sonication buffer (25 mM HEPES-NaOH pH 8.0, 0.5 M NaCl, 20 mM imidazole, 1 mM PMSF, protease inhibitor cocktail VII (Fisher Scientific)). The cells were disrupted by sonication, the lysate was clarified by centrifugation at 40000 g, 30 minutes, at 4°C, the soluble fraction was filtered through 0.22 µm diameter syringe filters (Sigma-Aldrich) and loaded onto a HisTrap Excel column (GE Healthcare), equilibrated in 25 mM HEPES-NaOH pH 8.0, 0.5 M NaCl, 20 mM imidazole. The column was washed extensively with the equilibration buffer and His-tagged eIF4A was eluted with a 10-column volume gradient of 20 mM – 1 M imidazole in the same buffer. Protein containing fractions were pooled, TEV protease was added at 1:20 (protein:TEV) mass ratio, followed by overnight dialysis against 25 mM HEPES-NaOH pH 8.0, 0.5 M NaCl, 20 mM imidazole at 4°C. The dialysed protein sample was then loaded onto a HisTrap Excel column (GE Healthcare) equilibrated in 25 mM HEPES-NaOH pH 8.0, 0.5 M NaCl, 20 mM imidazole. The flow-through was collected, spin concentrated, dialysed overnight at 4°C against 25 mM HEPES-NaOH pH 8.0, 100 mM NaCl, 10% v/v glycerol, aliquoted, frozen in liquid nitrogen and stored at -80°C. Purity was assessed by SDS PAGE and quantification was carried out spectrophotometrically.

Hippuristanol

A sample of hippuristanol was kindly provided by Professor Jerry Pelletier, Department of Biochemistry, McGill University, Canada.

Production of aryldiazirine salt

The sodium salt of TDBA (40 mM aqueous solution) was made by adding the required volume of aqueous NaOH (40 mM) to a 1.1 molar excess of solid TDBA. The suspension was agitated for 5 minutes and then incubated at room temperature for an hour before being centrifuged at 5000 g for 5 minutes. The supernatant was carefully removed and stored in a fresh 0.5 mL Eppendorf tube at 4°C.

Carbene footprinting

A volume of 1 μL of aqueous hippuristanol (280 μM) was added to 9 μL of eIF4A (14 μM) and incubated for 10 minutes. 10 μL of TDBA (40 mM) was combined with either ligand-treated or control samples and incubated for a further 10 minutes. 5 μL aliquots were transferred to autosampler vials (4 replicates) and flash-frozen with liquid nitrogen. Samples were irradiated using a Spectra Physics Explorer 349 laser (actively Q-switched Nd:YLF laser 349 nm wavelength, 1000 Hz repetition frequency, 125 μJ pulsed energy) that was vertically refracted into the vials by a 45° mirror.

Irradiated samples were combined with 6X loading dye (180 mM Tris-HCl pH 6.8, 12 % (w/v) SDS, 30% (v/v) glycerol, 0.15 % (w/v) bromophenol blue, 200 mM DTT) and incubated at 95°C for 10 minutes before being analysed with SDS-PAGE.

Proteolysis

eIF4A bands were excised using a scalpel, cut into 1 mm² pieces and destained with 50 μL acetonitrile solution (50%) for 10 minutes at room temperature. Gel pieces were dehydrated with 450 μL of acetonitrile (MeCN) with agitating for 3 minutes before the MeCN was removed. Gel pieces were treated with DTT solution to reduce protein disulfide bonds (DTT 10 mM, ammonium bicarbonate (AmBic) 100 mM) at 55°C for 30 minutes before being dehydrated with MeCN (450 μL). Gel pieces were then treated with iodoacetamide solution (iodoacetamide 55 mM, AmBic 100 mM) and incubated in the dark for 30 minutes to alkylate Cys thiol groups before again being dehydrated with MeCN (450 μL). Gel pieces were finally incubated with 50 μL of trypsin solution (10 ng / μL , AmBic 50 mM) at the 37°C for 18 hours.

Modelling of eIF4A

The closed model of eIF4A was generated by iTASSER server [40] with no specified template. Top models returned all matched to closed forms of eIF4AII. The best model was selected and templated onto a mix of PDB structures, including predominantly 2HYI (eIF4AIII) but also 2J0S, 5IVL, 4D25, 4C9B.

Liquid chromatography-mass spectrometry

1 μL of formic acid was added to protein digests and kept on ice. Supernatant was removed from the gel pieces and centrifuged at 5000 g for 5 minutes. This was transferred to plastic autosampler vials for nanoHPLC-MS analysis.

Digests were analysed with a Dionex U3000 nanoLC coupled to a ThermoFisher LTQ FT Ultra Mass Spectrometer containing a nano-ESI source. An injection volume of 3 μL was loaded onto a C18 Pepmap300 loading column (10 mm, 300 Å, 5 μm particle size). Sample separation was performed using a C18 Pepmap300 column (150 mm \times 75 μm , 300 Å, 5 μm particle size) with a gradient of two mobile phases: mobile phase A (5% acetonitrile, 0.1% formic acid) and mobile phase B (95% acetonitrile, 0.1% formic acid). The FT was operated in positive ion mode with a standard coated SilicaTip emitter nanospray source.

Quantification of carbene labelling was carried out in Pepfoot [17] using full scan mode files. Using unlabelled and labelled extracted ion chromatograms from the same peptide, spectral peaks were extracted - and depending on isotope distributions and mass accuracies - integrated, generating fractional modifications. Peptide identity was confirmed by CID MS/MS of precursor peptide ions and database searching using SearchGUI [41]. Raw data were deposited in the PRIDE database [42].

3 Results and Discussion

Differential footprinting of eIF4A was carried out by photochemical activation of the sodium salt of TDBA in the presence and absence of hippuristanol, as described in the Materials and Methods section. Following SDS-PAGE separation and proteolysis with trypsin, the extent of labelling on peptides was analysed by LC/MS. A total of 32 tryptic peptides corresponding to 67.2% coverage of eIF4A were identified. Of these 32 peptides, 12 displayed significant differences (Student's *t*-test, $P < 0.05$) in labelling between control and ligand-treated samples, with 6 of these peptides showing even greater significance (Student's *t*-test, $P < 0.01$).

Pleasingly, peptides predicted to contain residues involved in direct hippuristanol binding by NMR [34] displayed significant reductions in fractional modification (F_{mod}) by the carbene when hippuristanol was present (Figure 2). Peptide 335 – 353, whilst displaying very low labelling, showed a small but distinct masking event. Interestingly, when mapped onto the closed structure, the peptide occupied much of the cleft between domains. Indeed, this peptide contained part of the V motif, involved in RNA binding, inter-domain contact and ATP binding, as well as direct interaction with hippuristanol (Figure S1) [26]. The inherently more sequestered and consequently, shielded nature of this peptide may explain low levels of labelling in both samples with hippuristanol possibly contributing to further masking through direct steric inhibition or inducing closure of the protein. Nonetheless, the extent of eIF4A closure due to hippuristanol activity is unknown and whether residues involved in native inter-domain contacts reform these interactions remains undetermined. It does appear logical that disruption of residues involved in RNA interaction and proper inter-domain contact would impede nucleic acid binding and helicase functionality. Masking events were also observed at peptide 370 – 381 and the missed cleavage peptide 370 – 382, with the former showing higher significance than the latter. These were indicative of hippuristanol binding, and consistent with previous NMR data (Figure 3) [34].

Peptides predicted to be within 5Å of the hippuristanol binding site [34] also displayed changes in fractional modification in ligand-treated samples. Interestingly, peptide 238 – 247 displayed an unmasking event whilst the cleavage variant 239 – 247 exhibited a masking event. Both peptides formed part of the flexible linker region (Figure S1). This difference in labelling suggested that Lys₂₃₈ was relatively highly labelled in the ligand-bound state. As such, it can be envisioned that closure of eIF4A about the flexible linker caused conformational changes promoting unmasking and hence labelling at Lys₂₃₈. The N-terminus of eIF4A was not present in the construct used for the NMR study and so it was not possible to compare these effects with previous data [34]. Masking events on peptides 239 – 247, 248 – 255 and 325 – 334 were consistent with NMR data of the C-terminus, which predicted that residues on these peptides were located within 5Å of hippuristanol. It should be borne in mind that the relatively large size of the carbene probe will result in masking events occurring over a larger area than the direct contact surface of the ligand. Interestingly, peptide 325-334 contains part of the V motif, including Thr₃₂₉ which is implicated in RNA binding. Allosteric disruption of these conserved residues would likely hinder RNA interaction and eIF4A activity.

Indeed, Lindqvist and colleagues postulated that hippuristanol interfered with Thr₃₂₉ alignment, preventing interaction with RNA [34]. Masking events could not be observed for the previous peptide 320 – 335, suggesting that residues 320 – 324 were very highly labelled in the presence and absence of the ligand thereby concealing the masking event in peptide 320-335.

Several differences in labelling – both masking and unmasking events – were observed in peptides not seen in NMR data, including peptides 46 – 61, 69 - 82, 284 - 291, 296 – 309 and 296 – 311. Unmasking events were observed for both N-terminal peptides 46 – 61 and 69 – 82. However, the missed cleavage peptide 46 – 68 did not display similar labelling events despite sharing residues 46 – 61. This suggested that the subsequent residues 62 – 68 were highly labelled and influenced overall fractional modifications, consistent with our observations. This was further reinforced by peptide 62 – 82 displaying very high labelling ($F_{\text{mod}} \approx 1$), whilst peptide 69 – 82 displayed an overall reduction in labelling. Interestingly, both 46 – 61 and 69 – 82 contained conserved residues involved in ATP binding. Since hippuristanol is not thought to impede ATP binding [35] by masking implicated residues, this suggested the presence of the ligand induced conformational changes leading to higher probe insertion near or close to these residues. No NMR data were available for comparison here, as these residues were located in the N-terminal domain [34]. Peptides 296 – 309 and 296 – 311 were also of particular interest, containing residues from the QxxR motif that are thought to be involved in inter-domain contacts and RNA binding [26]. The observation of masking events at these peptides in ligand-treated samples supported the idea of hippuristanol triggering transition to some form of a closed structure in which RNA binding would be obstructed. Careful review of the NMR data from this region revealed a small but seemingly significant chemical shift perturbation around Asp₃₀₅ [34], which sits within peptides 296 – 309 and 296 – 311.

4 Concluding remarks

In summary, we have shown that differential carbene footprinting of the complete eIF4A construct with and without hippuristanol identifies the binding site to be within the protein's C-terminal domain, which is consistent with previous NMR work [34]. Further conformational changes associated with ligand interaction were also revealed for the first time. These were principally located around the flexible linker between the N- and C-terminal domains. The results demonstrate the feasibility of using carbene footprinting to understand and characterise protein-ligand interactions.

Acknowledgements

The authors are grateful to BBSRC for a studentship to JL.

Conflict of Interest

The authors declare no conflict of interest.

Supporting Information

Mass spectrometry raw data are being deposited to the ProteomeXchange Consortium (<http://proteomecentral.proteomexchange.org>) via the PRIDE partner repository [42] with the dataset identifier PXD025105.

Supporting information is available from the Wiley Online Library or from the author.

6 References

- [1] Yates, J. R. A century of mass spectrometry: from atoms to proteomes. (2011). *Nat. Methods*, 8(8), 633-637.
- [2] Eschweiler, J. D., Kerr R., Rabuck-Gibbons, J., & Ruotolo, B. T. Sizing Up Protein-Ligand Complexes: The Rise of Structural Mass Spectrometry Approaches in the Pharmaceutical Sciences. (2017). *Annu. Rev. Anal. Chem.*, 10: 25-44.
- [3] Mittermaier, A. & Kay, L. E. (2006). New Tools Provide New Insights in NMR Studies of Protein Dynamics. *Science*, 312, 224-228.
- [4] Pacholarz, K. J., Garlish, R A., Taylor, R. J., & Barran, P. E. (2012). Mass spectrometry based tools to investigate protein–ligand interactions for drug discovery. *Chem. Soc. Rev.*, 7, 4335-4355.
- [5] Zhang, Z. & Smith, D. L. (1993). Determination of amide hydrogen exchange by mass spectrometry: a new tool for protein structure elucidation. *Protein Sci.*, 2, 522-531.
- [6] Konermann, L., Pan, J. & Liu, Y. (2011). Hydrogen exchange mass spectrometry for studying protein structure and dynamics. *Chem. Soc. Rev.*, 40, 1224-1234.
- [7] Martens, C., Shekhar, M., Lau, A. M., Tajkhorshid, E. & Politis, A. (2019). Integrating hydrogen–deuterium exchange mass spectrometry with molecular dynamics simulations to probe lipid-modulated conformational changes in membrane proteins. *Nat. Protoc.*, 14, 3183-3204.
- [8] Wang, L. & Chance, M. R. (2011). Structural Mass Spectrometry of Proteins Using Hydroxyl Radical Based Protein Footprinting. *Anal. Chem.*, 83, 7234-7241.
- [9] Calabrese, A. N. Ault, J. R., Radford, S. E. & Ashcroft, A. E. (2015). Using hydroxyl radical footprinting to explore the free energy landscape of protein folding. *Methods*, 89, 38-44.
- [10] Li, K. S., Shi, L. & Gross, M. L. (2018). Mass Spectrometry-Based Fast Photochemical Oxidation of Proteins (FPOP) for Higher Order Structure Characterization. *Acc. Chem. Res.*, 51, 736-744.
- [11] Jumper, C. C. & Schreimer, D. C. (2011). Mass Spectrometry of Laser-Initiated Carbene Reactions for Protein Topographic Analysis. *Anal. Chem.*, 83, 2913-2920.
- [12] Limpikirati, P., Liu, T., & Vachet, R. W. (2018). Covalent labeling-mass spectrometry with non-specific reagents for studying protein structure and interactions. *Methods*, 144, 79-93.
- [13] Wang, L. & Chance, M. R. (2017). Protein Footprinting Comes of Age: Mass Spectrometry for Biophysical Structure Assessment. *Mol. Cell. Proteomics.*, 16, 706-716.
- [14] Jumper, C. C., Bomgarden, R., Rogers, J., Etienne, C., & Schriemer, D. C. (2012). High-Resolution Mapping of Carbene-Based Protein Footprints. *Anal. Chem.*, 84, 4411-4418.
- [15] Manzi, L., Barrow, A. S., Scott, D., Layfield, R., Wright, T. G., Moses, J. E. & Oldham, N. J. (2016). Carbene footprinting accurately maps binding sites in protein-ligand and protein-protein interactions. *Nat. Commun.*, 7, 1-9.
- [16] Manzi, L., Barrow, A. S., Hopper, J. T. S., Kaminska, R., Kleanthous, C., Robinson, C. V. ... Oldham, N. J. (2017). Carbene Footprinting Reveals Binding Interfaces of a Multimeric Membrane-Spanning Protein. *Angew. Chem. Int. Ed. Engl.*, 56, 14873-14877.
- [17] Bellamy-Carter, J. & Oldham, N. J. (2019). PepFoot: A Software Package for Semiautomated Processing of Protein Footprinting Data. *J. Proteome Res.*, 18, 2925-2930.

- [18] Jenner, M., Kosol, S., Griffiths, D., Prasongpholchai, P., Manzi, L., Barrow, A. S. ... Challis, G. L. (2018). Mechanism of intersubunit ketosynthase-dehydratase interaction in polyketide synthases. *Nat. Chem. Bio.*, 14, 270-275.
- [19] Lu, G., Xu, X., Li, G., Sun, H. (2019). Sub-residue Resolution Footprinting of Ligand-Protein Interactions by Carbene Chemistry and Ion Mobility-Mass Spectrometry. *Anal. Chem.*, 92, 947-956.
- [20] Chang, J. H., Cho, Y. H., Sohn, S. Y., Choi, J., Kim, A., Kim, Y. C. ... Cho, Y. (2009). Crystal structure of the eIF4A-PDCD4 complex. *Proc. Natl. Acad. Sci. U. S. A.*, 106, 3148-3153.
- [21] Li, Q., Imataka, H., Morino, S., Rogers, G. W. (1999). Eukaryotic Translation Initiation Factor 4AIII (eIF4AIII) Is Functionally Distinct from eIF4AI and eIF4AII. *Mol. Cell. Bio.*, 19, 7336-7346.
- [22] Uhlén, M., Fagerberg, L., Hallström, B. M., Lindskog, C., Oksvold, P., Mardinoglu, A. ... Pontén, F. (2015). Tissue-based map of the human proteome. *Science*, 347, 1260419.
- [23] Chan, C. C., Dostie, J., Diem, M. D., Feng, W., Mann, M., Rappsilber, J. & Dreyfuss, G. (2004). eIF4A3 is a novel component of the exon junction complex. *RNA*, 10, 200-209.
- [24] Jiang, C., Tang, Y., Ding, L., Tan, R., Li, X., Lu, J. ... Dang, Y. (2019). Targeting the N Terminus of eIF4AI for Inhibition of Its Catalytic Recycling. *Cell. Chem. Bio.*, 26, 1417-1426.
- [25] Anderson, C. B. F., Ballut, L., Johansen, J. S., Chamieh, H., Nielsen, K. H., Oliveira, C. L. P. (2006) Structure of the exon junction core complex with a trapped DEAD-box ATPase bound to RNA. *Science*, 313, 1968-1972.
- [26] Sengoku, T., Nureki, O., Nakamaru, A., Kobayashi, S., Yokoyama, S. (2006). Structural basis for RNA unwinding by the DEAD-box protein *Drosophila* Vasa. *Cell*, 125, 287-300.
- [27] Theissen, B., Karow, A. R., Köhler, J., Gubaev, A. & Klostermeier, D. (2008). Cooperative binding of ATP and RNA induces a closed conformation in a DEAD box RNA helicase. *Proc. Natl. Acad. U. S. A.*, 105, 548-553.
- [28] Lorsch, J. R. & Herschlag, D. (1998). The DEAD Box Protein eIF4A. 2. A Cycle of Nucleotide and RNA-Dependent Conformational Changes. *Biochemistry*, 37, 2194-2206.
- [29] Querido, J. B., Sokabe, M., Kraatz, S., Gordyenko, Y., Skehel, J. M., Fraser, C. S. & Ramakrishnan, V. (2020). Structure of a human 48S translational initiation complex. *Science*, 369, 1220-1227.
- [30] Rogers Jr, G. W., Richter, N. J., Lima, W. F. & Merrick, W. C. (2001). Modulation of the helicase activity of eIF4A by eIF4B, eIF4H, and eIF4F. *J. Biol. Chem.*, 276, 30914-30922.
- [31] Takyar, S., Hickerson, R. P. & Noller, H. F. (2005). mRNA Helicase Activity of the Ribosome. *Cell*, 120, 49-58.
- [32] Jackson, R.J., Hellen, C. U. T., Pestova, T. V. (2010). The mechanism of eukaryotic translation initiation and principles of its regulation. *Nat. Rev. Mol. Cell Biol.*, 11, 113-127.
- [33] Pestova, T. V. & Hellen, C. U. T. (2006). Small molecule derails translation initiation. *Nat. Chem. Biol.*, 2, 176-177.
- [34] Lindqvist, L., Oberer, M., Reibarkh, M., Cencic, R., Bordeleau, M., Vogt, E. ... Pelletier, J. (2008). Selective Pharmacological Targeting of a DEAD Box RNA Helicase. *PLoS One.*, 3, e1583.

- [35] Cencic, R. & Pelletier, J. (2016). Hippuristanol - A potent steroid inhibitor of eukaryotic initiation factor 4A. *Translation*, 4, e1137381.
- [36] Sun, Y., Atas, E., Lindqvist, L. M., Sonenberg, N., Pelletier, J. & Meller, A. (2014). Single-molecule kinetics of the eukaryotic initiation factor 4A1 upon RNA unwinding. *Structure*, 22, 941-948.
- [37] Cramer, Z., Sadek, J., Galicia-Vázquez, G., Marco, S. D. Pause, A., Pelletier, J. & Gallouzi, I. (2018). eIF4A inhibition prevents the onset of cytokine-induced muscle wasting by blocking the STAT3 and iNOS pathways. *Sci. Rep.*, 8, 8414.
- [38] Cencic, R., Robert, F., Galicia-Vázquez, G., Malina, A., Ravindar, K., Somaiah, R. ... Pelletier, J. (2013). Modifying chemotherapy response by targeted inhibition of eukaryotic initiation factor 4A. *Blood Cancer J.*, 3, e128.
- [39] Ishikawa, C., Tanaka, J., Katano, H., Senba, M. & Mori, N. (2013). Hippuristanol Reduces the Viability of Primary Effusion Lymphoma Cells both in Vitro and in Vivo. *Mar. Drugs*, 11, 3410-3424.
- [40] Yang, J., Yan, R., Roy, A., Xu, D., Poisson, J. & Zhang, Y. (2015). The I-TASSER Suite: protein structure and function prediction. *Nat. Methods*, 12, 7-8.
- [41] Barsnes, H. & Vaudel, M. (2018). SearchGUI: a highly adaptable common interface for proteomics search and de novo engines. *J. Proteome Res.*, 17, 2552-2555.
- [42] Perez-Riverol, Y., Csordas, A., Bai, J., Bernal-Llinares, M., Hewapathirana, S., Kundu, D. J. ... Vizcaíno, J. A. (2019). The PRIDE database and related tools and resources in 2019: improving support for quantification data. *Nucleic Acids Res.*, 47, D442-D450.

Figures

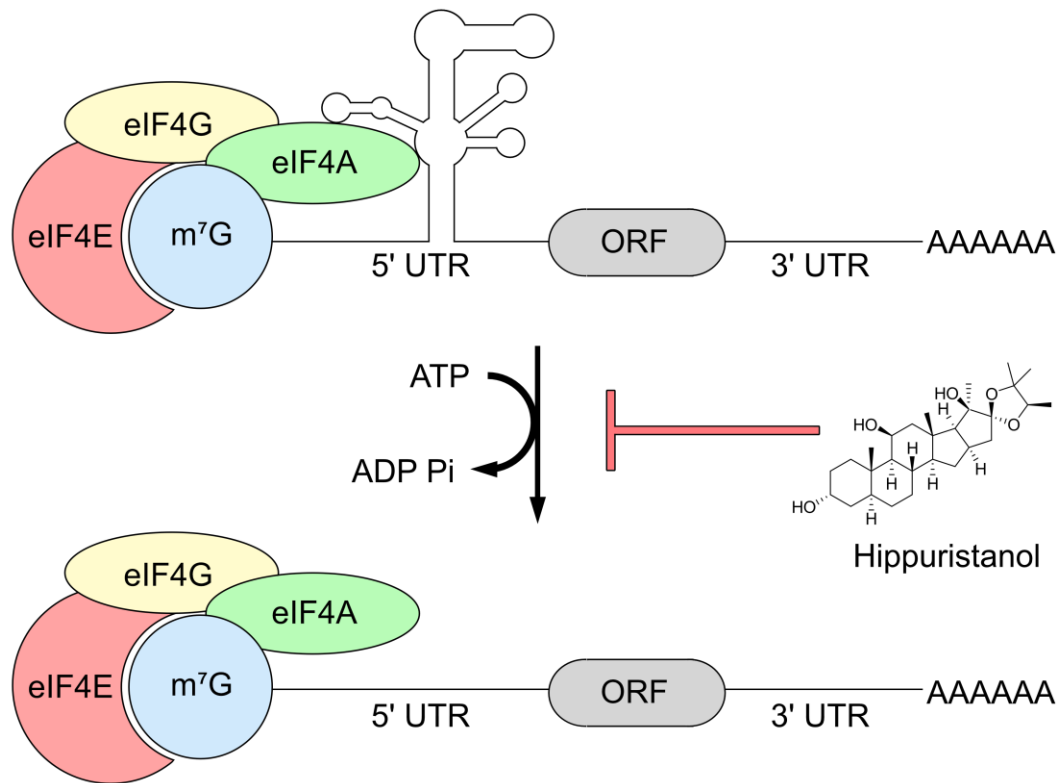
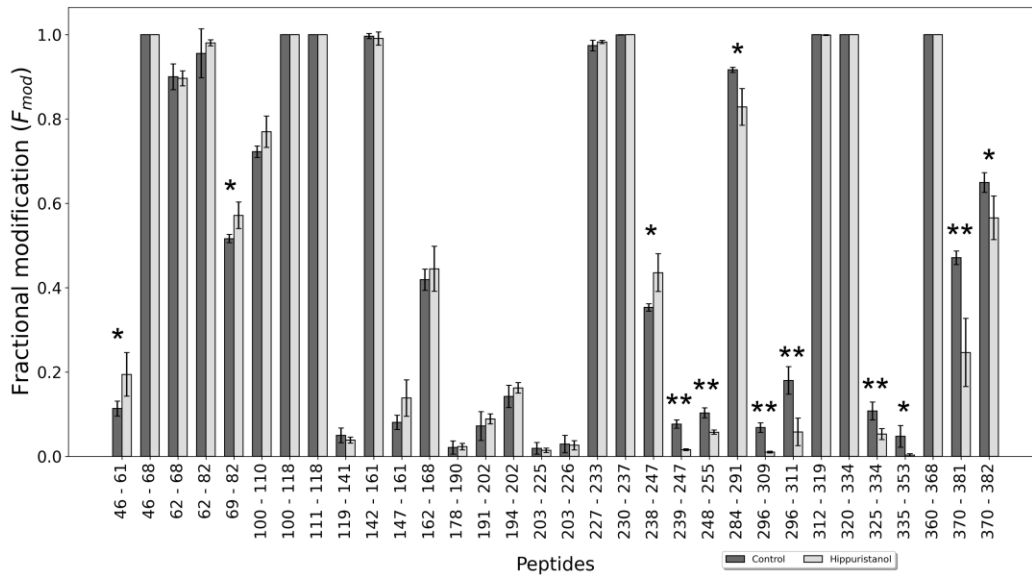


Figure 1. eIF4A-mediated unwinding of 5' UTR higher-order structures as part of the eIF4F complex and inhibition of this process by hippuristanol.

(a)



(b)

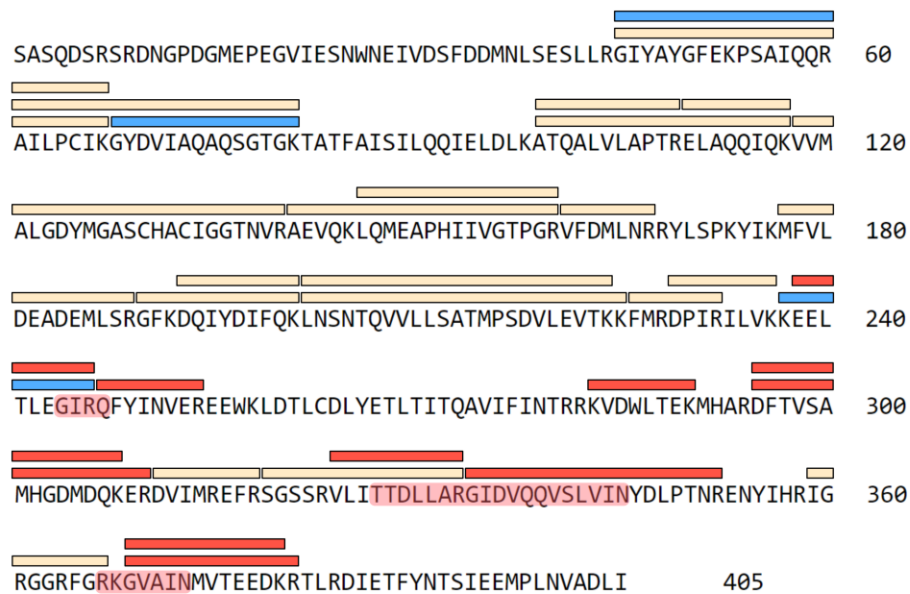


Figure 2. Carbene footprinting of eIF4A and hippuristanol. (a) Fractional modification of eIF4A peptides in the presence (light grey) and absence (dark grey) of hippuristanol. Error bars are \pm standard deviation ($n = 4$). Significant difference between samples is highlighted with either * (Student t -test, $P < 0.05$) or ** (Student t -test, $P < 0.01$). (b) Observed tryptic peptides mapped onto the eIF4A sequence with bars below indicating significant ($P < 0.05$) masking events (red), significant ($P < 0.05$) unmasking events (blue) and no differences (wheat). Highlighted residues (red) indicate predicted regions involved in hippuristanol binding [34]. Sequence numbering is consistent with previous studies.

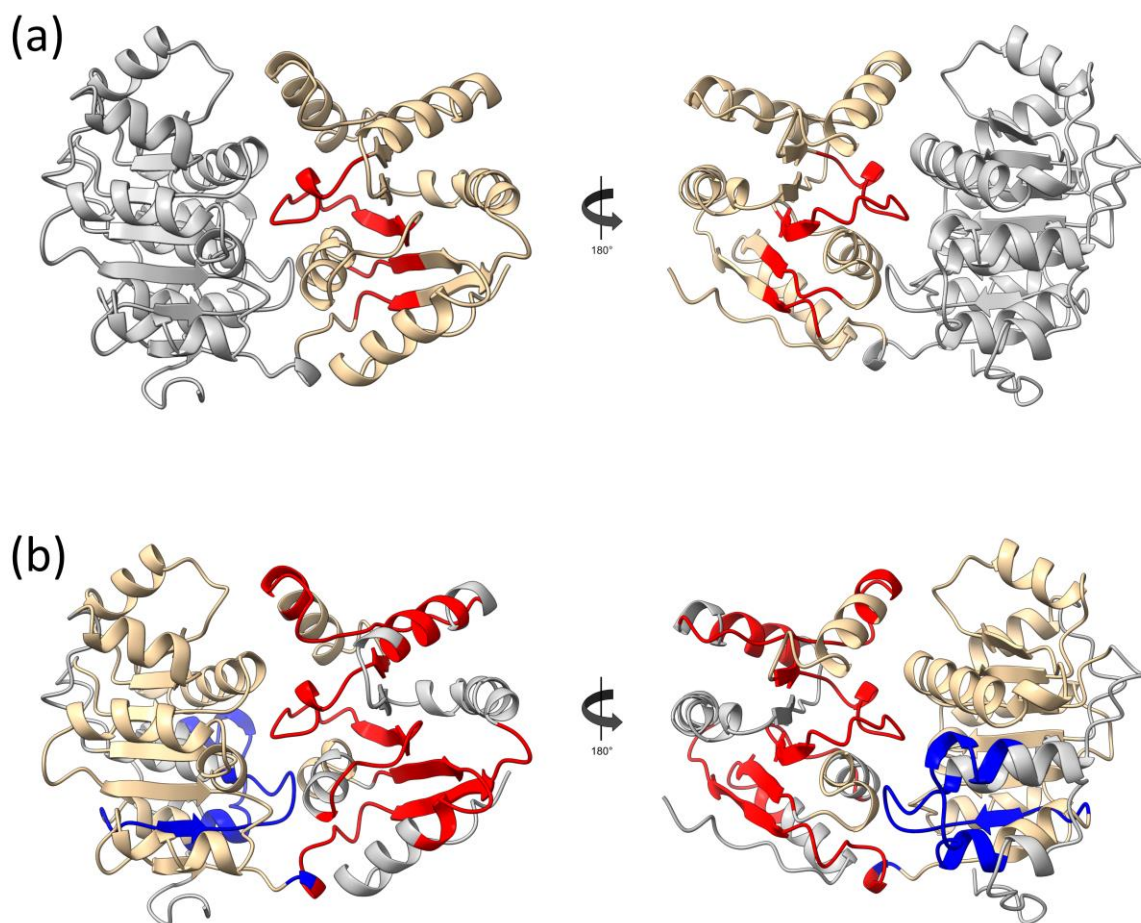


Figure 3. Model of the closed structure of eIF4A highlighted according to: a) NMR data; residues predicted to be involved in hippuristanol binding (red) [34]; b) Carbene footprinting data; peptides showing significant masking ($P < 0.05$) (red) or unmasking (blue) due to the presence of hippuristanol. In both cases, regions coloured in wheat show no difference due to hippuristanol, and those coloured grey indicate no coverage.